PHYSICAL REVIEW D **96,** 055022 (2017)

Neutrino-two-Higgs-doublet model with the inverse seesaw mechanisms

Yi-Lei Tang*
Center for High Energy Physics, Peking University, Beijing 100871, China

Shou-hua Zhu†
Institute of Theoretical Physics & State Key Laboratory of Nuclear Physics and Technology, Peking University, Beijing 100871, China; Collaborative Innovation Center of Quantum Matter, Beijing 100871, China; and Center for High Energy Physics, Peking University, Beijing 100871, China
(Received 21 March 2017; published 19 September 2017)

In this paper, we combine the ν-two-Higgs-doublet-model with the inverse seesaw mechanisms. In this model, the Yukawa couplings involving the sterile neutrinos and the exotic Higgs bosons can be of order 1 in the case of a large $\tan\beta$. We calculated the corrections to the Z-resonance parameters R_{l_i}, A_{l_i}, and N_ν, together with the $l_1 \to l_2\gamma$ branching ratios and the muon anomalous $g-2$. Compared with the current bounds and plans for the future colliders, we find that the corrections to the electroweak parameters can be constrained or discovered in much of the parameter space.

DOI: 10.1103/PhysRevD.96.055022

I. INTRODUCTION

The smallness of the neutrino masses can be explained by the seesaw mechanisms. In the framework of the type-I seesaw mechanisms [1–5], large Majorana masses ($\sim M_N$) are introduced for the right-handed neutrinos. The Yukawa couplings (y_DLHN) between the left-handed and the right-handed neutrinos through a Higgs doublet generate the Dirac mass terms ($\sim m_D = y_D v$). After "integrating out" the right-handed neutrinos, or equivalently diagonalizing the full neutrino mass matrix, one obtains the tiny neutrino masses ($\sim \frac{m_D^2}{M_N}$) suppressed by the M_N in the denominator.

The standard seesaw mechanisms usually require extremely large $M_N \sim 10^{9-13}$ GeV in the case in which the Yukawa coupling constant $y_D \sim 0.01$–1, which is beyond the scope of any realistic collider proposal. An alternative scheme to lower the sterile neutrino masses down to the 100–1000 GeV scale without introducing too-small Yukawa coupling constants is the "inverse seesaw" mechanisms (see Refs. [6–9] for the early works and Ref. [10] for a recent model discussion). In the inverse seesaw mechanisms, pairs of the Weyl spinors charged with the lepton number (L) form the pseudo-Dirac neutrinos ($N_{L,R}$). Small Majorana mass terms ($\sim \mu \bar{N}_L N_L^c$) that softly break the lepton number are introduced, as are the lepton-number-conserving Dirac mass terms ($\sim m_N \bar{N}_L N_R$). Again, after integrating out the sterile neutrinos, or equivalently diagonalizing the full neutrino mass matrix, one finds the tiny neutrino masses ($\sim \frac{m_D^2}{m_N^2}\mu$). Thus, the smallness of the neutrino masses is explained by the smallness of the μ.

Compared with the standard TeV-scale seesaw mechanisms, the mixings between the left-handed and sterile neutrinos can be much larger in the inverse seesaw mechanisms. This offers us some possibilities to test or constrain the models by the collider experiments. However, the LHN$_D$ Yukawa couplings should still be well below the order of 1 due to various constraints. One way to raise the Yukawa coupling constants of the neutrinos is the ν-two-Higgs-doublet model (νTHDM). (For some early works, see Refs. [11,12]. For some discussions of the collider physics, see Refs. [13,14]. For some variants, see Refs. [15–18]. Reference [19] also proposed an interesting picture to understand the extra Higgs bosons through the neutrino condensation.) This is a variant of the type-I two-Higgs-doublet model (for a review of the THDM, see Ref. [20] and references therein). In this model, all the standard model fermions couple with one of the Higgs doublet (usually named Φ_2), while the neutrino sector couples with the other (Φ_1). The Yukawa coupling constants of the neutrino sector are then amplified by a factor of $\sec\beta \approx \tan\beta = \frac{v_2}{v_1}$. In the usual cases of the νTHDM, we need a $\tan\beta \gtrsim 10^4$ for a Yukawa coupling of order 1. In fact, in the THDM with the exact Z_2 symmetry, there is a strong constraint on $\tan\beta$ due to the unitarity and the stability of the scalar potential [21–23]. A softly broken Z_2 symmetry by a m_{12}^2 will relax such constraints, and in Ref. [24], the author also mentioned that the scenario of $\tan\beta \gg 1$ is perturbatively reliable. However, if we combine the νTHDM with the inverse seesaw mechanisms, a $\tan\beta \sim 10^{2-3}$ is enough.

The relatively large Yukawa coupling constants will not only provide the opportunities of directly observing the sterile neutrinos in the future collider experiments but will also affect the electroweak observables. In this paper, we

*tangyilei15@pku.edu.cn
†shzhu@pku.edu.cn

concentrate on the Z-resonance observables R_l and A_l, where l=e, μ, τ (besides the corresponding chapters in Ref. [25], see Refs. [26–30] for details and Ref. [31] for a theoretical point of view). We also consider the leptonic flavor-changing neutral current (FCNC) $l_1 \to l_2 + \gamma$ decay bounds and the muon anomalous magnetic moment. We will show that in some of the parameter space it is possible for the future collider experiments to detect the small deviations on Z-resonance observables originated from this model.

II. MODEL DESCRIPTIONS

To start, we shall make a brief review of the THDM. The Higgs potential is given by

$$\begin{aligned} V = {} & m_1^2\Phi_1^\dagger\Phi_1 + m_2^2\Phi_2^\dagger\Phi_2 - m_{12}^2(\Phi_1^\dagger\Phi_2 + \Phi_2^\dagger\Phi_1) \\ & + \frac{\lambda_1}{2}(\Phi_1^\dagger\Phi_1)^2 + \frac{\lambda_2}{2}(\Phi_2^\dagger\Phi_2)^2 \\ & + \lambda_3(\Phi_1^\dagger\Phi_1)(\Phi_2^\dagger\Phi_2) + \lambda_4(\Phi_1^\dagger\Phi_2)(\Phi_2^\dagger\Phi_1) \\ & + \frac{\lambda_5}{2}[(\Phi_1^\dagger\Phi_2)^2 + (\Phi_2^\dagger\Phi_1)^2], \end{aligned} \tag{1}$$

where $\Phi_{1,2}$ are the two Higgs doublets with hypercharge $Y = \frac{1}{2}$; λ_{1-7} are the coupling constants; and m_1^2, m_2^2, and m_{12}^2 are the mass parameters. As in most of the cases in the literature, we impose a Z_2 symmetry that $\Phi_i \to (-1)^{i-1}\Phi_i$ to avoid the tree-level FCNC. This symmetry forbids the $[\lambda_6(\Phi_1^\dagger\Phi_1) + \lambda_7(\Phi_2^\dagger\Phi_2)](\Phi_1^\dagger\Phi_2 + \text{H.c.})$ terms and is softly broken by the m_{12}^2 term.

After the electroweak symmetry breaking, the Higgs doublets acquire the vacuum expectation values (VEVs) $v_{1,2}$, and the Higgs component fields form physical mass eigenstates $H^\pm$, h, H, and A as well as the Goldstone bosons $G^{\pm,0}$,

$$\begin{aligned} \Phi_1 = {} & \frac{1}{\sqrt{2}}\begin{pmatrix} \sqrt{2}(G^+\cos\beta - H^+\sin\beta) \\ v\cos\beta - h\sin\alpha + H\cos\alpha + i(G^0\cos\beta - A\sin\beta) \end{pmatrix}, \\ \Phi_2 = {} & \frac{1}{\sqrt{2}}\begin{pmatrix} \sqrt{2}(G^+\sin\beta + H^+\cos\beta) \\ v\sin\beta + h\cos\alpha + H\sin\alpha + i(G^0\sin\beta + A\cos\beta) \end{pmatrix}, \end{aligned} \tag{2}$$

where $\tan\beta = \frac{v_2}{v_1}$ and α is the mixing angle between the CP-even states. Note that in this paper we ignore the CP effects in the scalar sector. Therefore, λ_{1-5} and also m_1^2, m_2^2, and m_{12}^2 are real numbers, and there is no mixing between the CP-even Higgs bosons H and h and the CP-odd Higgs boson A.

The type-I THDM is characterized by coupling all the standard model (SM) fermions Q_L, u_R, d_R, L_L, and e_R with the Φ_2 field

$$\begin{aligned} \mathcal{L}_{\text{Yukawa}}^{\text{SM}} = {} & -Y_{uij}\bar{Q}_{Li}\tilde{\Phi}_2 u_{Rj} - Y_{dij}\bar{Q}_{Li}\Phi_2 d_{Rj} \\ & - Y_{lij}\bar{L}_{Li}\Phi_2 l_{Rj} + \text{H.c.}, \end{aligned} \tag{3}$$

where $Y_{u,d,l}$ are the 3×3 coupling constants. This can be achieved by charging all the right-handed fields with the -1 and the left-handed fields with the $+1$ under the Z_2 symmetry described above. In the limit that $\tan\beta \to \infty$ and $\sin(\beta-\alpha) \to 1$, the couplings between the SM fermions and the exotic Higgs bosons (H, A, $H^\pm$) are highly suppressed by $\sin\alpha$ or $\frac{1}{\tan\beta}$, making them easy to evade various bounds.

Based on the type-I THDM, if we introduce the sterile neutrinos N and charge them with $+1$ under the Z_2 symmetry, we get the νTHDM. In the νTHDM, sterile neutrinos couple with the L_L only through the Φ_1. Since in this paper we will combine the inverse seesaw mechanisms with the νTHDM, we then introduce three pairs of sterile neutrino fields $N_{Li} = P_L N$, $N_{Ri} = P_R N$ charged with the lepton number 1, where $i = 1-3$, $P_{L,R} = \frac{1\mp\gamma^5}{2}$, and the Dirac 4-spinors N_i can be written in the form of $\begin{bmatrix} N_{Li}^{\text{w}} \\ i\sigma^2 N_{R_i}^{\text{w}*} \end{bmatrix}$. The corresponding Lagrangian is given by

$$\mathcal{L}_{\text{Yukawa}}^{\nu} = -Y_{Nij}\bar{L}_{Li}\tilde{\Phi}_1 N_{Rj} - m_{Nij}\bar{N}_{Li}N_{Rj} - \mu_{ij}\overline{N_{Li}^c}N_{Lj}, \tag{4}$$

where Y_N is the 3×3 Yukawa coupling constant matrix, m_N is the 3×3 Dirac mass matrix between the sterile neutrino pairs, mu is a 3×3 mass matrix which softly breaks the lepton number, and $N_{Li}^c = -i\gamma^2\gamma^0\overline{N_{Li}^c}^T$ is the charge conjugate transformation of the N_{Li} field.

The VEV of the Φ_1 contributes to the Dirac mass terms between the left-handed neutrinos and the sterile neutrinos,

$$m_D = \frac{v_1}{\sqrt{2}}Y_N. \tag{5}$$

The full 9×9 mass matrix among the Weyl 2-spinors ν_L^{w}, N_L^{w}, and N_R^{w} is given by

$$M = \begin{bmatrix} 0 & m_D & 0 \\ m_D^T & 0 & m_N \\ 0 & m_N^T & \mu \end{bmatrix}. \tag{6}$$

Now, we will try to diagonalize (6). Define the 9×9 matrix

$$V = \begin{bmatrix} I & 0 & V_{13} \\ 0 & I & 0 \\ V_{13}^\dagger & 0 & I \end{bmatrix}, \tag{7}$$

where V_{13} is the 3×3 matrix that is used to mix the ν_L^{w} and N_L^{w}. We should also note that the elements of $|V_{13}|_{ij} \ll 1$ so that (7) is an approximation of a unitary matrix. Calculating the VMV^T results in

$$VMV^T = \begin{bmatrix} V_{13}\mu V_{13}^T & m_D + V_{13} m_N^T & V_{13}\mu \\ m_D^T + m_N V_{13}^T & 0 & -m_D^T V_{13}^* + m_N \\ \mu V_{13}^T & -V_{13}^\dagger m_D + m_N^T & \mu \end{bmatrix}. \tag{8}$$

Therefore, $V_{13} = -m_D (m_N^T)^{-1}$ will lead to

$$VMV^T = \begin{bmatrix} m_D (m_N^T)^{-1} \mu m_N^{-1} m_D^T & 0 & V_{13}\mu \\ 0 & 0 & -m_D^T V_{13}^* + m_N \\ \mu V_{13}^T & -V_{13}^\dagger m_D + m_N^T & \mu \end{bmatrix}. \tag{9}$$

Further diagonalizing (9) requires diagonalizing the submatrix

$$\begin{bmatrix} 0 & -m_D^T V_{13}^* + m_N \\ -V_{13}^\dagger m_D + m_N^T & \mu \end{bmatrix}, \tag{10}$$

and then a standard seesaw mechanism can be applied in the final step. However, it is easy to see that this will only lead to a subleading correction of $\sim V_{13}^2 \mu^2 m_N^{-1}$ to the upper-left elements $m_D (m_N^T)^{-1} \mu m_N^{-1} m_D^T$. Thus, the light neutrino mass matrix is given by

$$m_D (m_N^T)^{-1} \mu m_N^{-1} m_D^T. \tag{11}$$

Diagonalizing (11), we need the Pontecorvo–Maki–Nakagawa–Sakata (PMNS) matrix

$$U = \begin{bmatrix} c_{12}c_{13} & s_{12}c_{13} & s_{13}e^{-i\delta} \\ -s_{12}c_{23} - c_{12}s_{23}s_{13}e^{i\delta} & c_{12}c_{23} - s_{12}s_{23}s_{13}e^{i\delta} & s_{23}c_{13} \\ s_{12}s_{23} - c_{12}c_{23}s_{13}e^{i\delta} & -c_{12}s_{23} - s_{12}c_{23}s_{13}e^{i\delta} & c_{23}c_{13} \end{bmatrix} \times \mathrm{diag}(1, e^{i\frac{\alpha_{21}}{2}}, e^{i\frac{\alpha_{31}}{2}}),$$
$$\mathrm{diag}(m_1, m_2, m_3) = U^T m_\nu U, \tag{12}$$

where $s_{ij} = \sin\theta_{ij}$, $c_{ij} = \cos\theta_{ij}$, and θ_{ij} are the mixing angles; δ is the CP-phase angle; and $\alpha_{21,31}$ are the two Majorana CP phases. $m_{1,2,3}$ are the masses of the three light neutrinos. Part of the parameters has been measured, and in the rest of this paper, we adopt the following central value [32]:

$$\begin{aligned} \Delta m_{21}^2 &= 7.37\ \mathrm{eV}^2, \\ |\Delta m^2| &= \left|\Delta m_{32}^2 + \Delta \frac{m_{21}^2}{2}\right| = 2.50\ \mathrm{eV}^2, \\ \sin\theta_{12}^2 &= 0.297 \\ \sin^2\theta_{23} &= 0.437, \\ \sin^2\theta_{13} &= 0.0214. \end{aligned} \tag{13}$$

We set all the CP phases as zero for simplicity.

To understand the approximate tri-bi-maximal structure of the U as the θ_{13} is relatively small compared with other mixing angles, models [33,34] have been built by introducing some flavon fields. Table I in Ref. [33] listed seven cases of different m_D, m_N, and μ combinations in such kinds of models. In this paper, we only discuss the previous three cases. They are listed in Table I. Unlike Ref. [33], here, M_0 should be compatible with a nonzero θ_{13}, just as the example revealed in Ref. [34].

TABLE I. Possible m_D, m_N, and μ combinations. Here, M_0 means a matrix that is not proportional to the identical matrix I.

Cases	1	2	3
m_D	M_0	$\propto I$	$\propto I$
m_N	$\propto I$	M_0	$\propto I$
μ	$\propto I$	$\propto I$	M_0

Define

$$m_\nu^{\frac{1}{2}} = U \cdot \mathrm{diag}(\sqrt{m_1}, \sqrt{m_2}, \sqrt{m_3}) \tag{14}$$

so that $m_\nu^{\frac{1}{2}} (m_\nu^{\frac{1}{2}})^T = m_\nu$. Therefore, during the numerical calculation processes, we set

$$m_D \propto m_\nu^{\frac{1}{2}}, \qquad m_N^{-1} \propto I, \qquad \mu \propto I \tag{15}$$

in case 1,

$$m_D \propto I, \qquad m_N^{-1} \propto (m_\nu^{\frac{1}{2}})^T, \qquad \mu \propto I \tag{16}$$

in case 2, and

$$m_D \propto I, \qquad m_N^{-1} \propto I, \qquad \mu \propto m_\nu \tag{17}$$

in case 3. Note that the definition in (14) of the $m_\nu^{\frac{1}{2}}$ is not the only one that can reach $m_\nu^{\frac{1}{2}} (m_\nu^{\frac{1}{2}})^T = m_\nu$. However, all the other definitions can be equivalent with (14) by redefining the $N_{L,R}$ fields, so it is enough to adopt (15)–(17) in all three cases.

III. CALCULATIONS OF THE OBSERVABLES

The Z-boson mass m_Z, the Fermi constant G_F, and the fine structure constant α are the three parameters with the smallest experimental errors. Together with the strong

coupling constant α_s, the SM-Higgs boson mass m_h, and the fermion masses and mixings, these parameters can be used as the input parameter set to evaluate other observables. Reference [25] states that their fits of the "SM values" are not the practical consequences for the precisely known α, G_F, and m_Z. However, in principle, we can always calculate the "SM-predicted" values of the observables from the parameters listed above and compare them with the measured ones on various (proposed future) experiments.

In this paper, we mainly discuss Z-resonance observables. They are $R_l = \frac{\Gamma_{Z\to\text{hadrons}}}{\Gamma_{Z\to l^+l^-}}$ and $A_l = \frac{2\bar{g}_V^l \bar{g}_A^l}{\bar{g}_V^{l2}+\bar{g}_A^{l2}}$. The muon's anomalous magnetic moment $g-2$, the lepton's FCNC decay $\tau \to e/\mu + \gamma$, $\mu \to e + \gamma$ are also calculated. All the SM input parameters can be measured independently from these observables. For example, the Fermi constant G_F can be extracted from the precisely measured muon mass and its lifetime [35], the current value of the fine structure constant α originates from low-energy experiments, and the $\hat{\alpha}(m_Z)$ defined in the modified minimal subtraction ($\bar{\text{MS}}$) is then calculated by considering the vacuum polarization effects of the leptons and hadrons (in Ref. [25], there is a review; see also the references therein). Another example is the α_s, which can be extracted from the R_l, though there are various other measures to acquire its value that can reach at least similar precision.

In some cases, the new physics sectors might shift the values of the SM input parameters, altering the SM-predicted values of some observables. In this paper, we should note that the decay width $\Gamma_{\mu\to e\nu\bar{\nu}}$ can be affected by the $H^\pm$ mediator, shifting the measured Fermi constant G_F from its "real value." We consider this effect in our following discussions; however, we do not care about the breaking of lepton universality of the "flavorful" gauge couplings $g_{e,\mu,\tau}$ (for an example, see Ref. [16], and see Ref. [36] for the experimental results) at the moment in this paper.

To calculate the shift of the decay width of the muon, we need to diagonalize the m_N matrix beforehand. Suppose m_N has been diagonalized and m_N^i's are the eigenvalues of this matrix; then, the shift to the muon's decay width is given by [15,37]

$$\Gamma_\mu = \Gamma_{\mu,\text{SM}}\left[1+\left(\frac{v}{\sqrt{2}m_{H^\pm}^4}\right)^4 \frac{\sum_{i=1-3,l=e,\mu,\tau} U_{li}^{\nu N} Y_{Nei} \sum_{j=1-3,l'=e,\mu,\tau}^{3} U_{l'j}^{\nu N} Y_{N\mu j}}{4}\right], \tag{18}$$

where $U^{\nu N}$ is the mixing between the light neutrinos and the sterile neutrinos. If m_N is diagonalized beforehand, then $U^{\nu N} = V_{13}$, where V_{13} is the submatrix of V when diagonalizing (6). Then, the shift of the G_F can be estimated as

$$\begin{aligned} &G_F \to G_F + \delta G_F, \\ &\delta G_F \approx G_F\left(\frac{v}{\sqrt{2}m_{H^\pm}^4}\right)^4 \frac{\sum_{i=1-3,l=e,\mu,\tau} U_{li}^{\nu N} Y_{Nei} \sum_{j=1-3,l'=e,\mu,\tau}^{3} U_{l'j}^{\nu N} Y_{N\mu j}}{8}. \end{aligned} \tag{19}$$

The values of the $U^{\nu N}$'s are calculated to be

$$U_{l,i}^{\nu N} = -\frac{Y_{Nli} v \cos\beta}{m_{Ni}}. \tag{20}$$

Notice that some of the tree-level definitions of the electroweak observables are functions depending only on the weak mixing angle θ_W. Therefore, we need to calculate the shifting of the θ_W,

$$\begin{aligned} &\frac{8G_F M_Z}{\sqrt{2}e^2} = \frac{1}{\sin^2\theta_W \cos\theta_W}, \\ &\to \delta\theta_W = \frac{8\delta G_F M_Z}{\sqrt{2}e^2}\left(\frac{-2}{\sin^3\theta_W} + \frac{1}{\sin\theta_W\cos^2\theta_W}\right). \end{aligned} \tag{21}$$

Now, we are ready to calculate

$$\begin{aligned} \delta R_l &= R_l^{\text{exp}} - R_l^{\text{SM Pre}}, \\ \delta A_l &= A_l^{\text{exp}} - A_l^{\text{SM Pre}}, \\ \delta N_\nu &= N_\nu^{\text{exp}} - 3, \end{aligned} \tag{22}$$

where

$$\begin{aligned} R_{l_i} &= \frac{\Gamma_{Z\to\text{had}}}{\Gamma_{Z\to l_i^+ l_i^-}} \\ A_{l_i} &= \frac{2\bar{g}_V^{l_i}\bar{g}_A^{l_i}}{\bar{g}_V^{l_i 2}+\bar{g}_A^{l_i 2}}. \end{aligned} \tag{23}$$

The superscript "exp." indicates the experimentally measured values, and the superscript "SM Pre." indicates the SM-predicted values in which the shifting of the Fermi

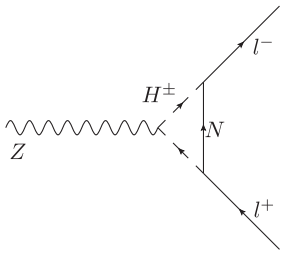

FIG. 1. (a) to the $Z - l^+ - l^0$ vertices.

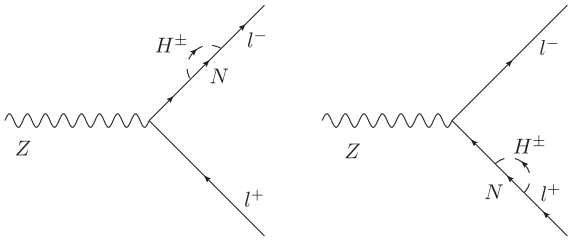

FIG. 2. (c) Diagrams to $l^\pm$ propagators.

constant G_F is taken into account. The definitions of the N_ν are a little bit complicated and will be discussed later. All of the δX's involve the corrections to the effective coupling constants $\bar{g}^{ffZ}_{A,V,L,R}$'s defined by

$$\begin{aligned}\mathcal{L}_{ffZ} &= \frac{-e}{2\sin\theta_W\cos\theta_W} Z_\mu \bar{f}\gamma^\mu \left[\bar{g}^f_L \frac{1-\gamma^5}{2} + \bar{g}^f_R \frac{1+\gamma^5}{2}\right] f \\ &= \frac{-e}{2\sin\theta_W\cos\theta_W} Z_\mu \bar{f}\gamma^\mu (\bar{g}^f_V - \bar{g}^f_A\gamma^5) f, \end{aligned} \tag{24}$$

where

$$\bar{g}^f_V = \bar{g}^f_L + \bar{g}^f_R, \qquad \bar{g}^f_A = \bar{g}^f_L - \bar{g}^f_R \tag{25}$$

and

$$\bar{g}^f_{L,R,V,A} = g^f_{L,R,V,A} + \delta g^f_{L,R,V,A}, \tag{26}$$

where $g^f_{L,R,V,A}$ are the SM values and the $\delta g^f_{L,R,V,A}$ are the new physics corrections.

To calculate the $Z - l^+ - l^-$ loop corrections where $l = e, \mu, \tau$, we need to calculate the Feynmann diagrams in Figs. 1 and 2. Reference [38] calculated the loop corrections to the $Z - b - b$ vertices, and it is easy to modify the formulas there to evaluate the Z vertices in this paper. Suppose m_N have been diagonalized; we have

$$\begin{aligned}\delta g^{l_1 l_2 (a)}_L &= \frac{1}{8\pi^2} Y_{Nl_1 j} Y^*_{Nl_2 j} g^{ZH^+H^-}_L C_{00}(0,0,m^2_Z, m^2_{H^\pm}, m^2_{Ni}, m^2_{H^\pm}), \\ \delta g^{l_1 l_2 (c)}_L &= \frac{1}{16\pi^2} y_{Nl_1 j} Y^*_{Nl_2 j} g^{Zl^+_1 l^-}_L B_1(0, |m_{Ni}|^2, m^2_{H^\pm}), \\ \delta g^{l_1 l_2}_L &= \delta g^{l_1 l_2 (a)}_L + \delta g^{l_1 l_2 (c)}_L, \\ \delta g^{l_1 l_2}_R &= 0 \end{aligned} \tag{27}$$

for lepton l_1 and l_2. C_{ij} and B_i are the Passarino-Veltman integrals with the conventions of the parameters similar to the LoopTools manual [39]. We also ignore all the leptonic masses during the calculations. Notice that if $l_1 \neq l_2$ the (27) can result in a FCNC $Z \to l_1 l_2$ decay. In this paper, we are not going to talk about them since they are exceeding the abilities of many collider experiments if $\mu \to e\gamma$ bounds are also considered, which is similar to the cases described in Ref. [16].

The $Z \to \nu\nu$ vertices also receive loop corrections. By calculating the Feynmann diagrams in Figs. 3 and 4, we have

$$\begin{aligned}\delta g^{\nu_{l1}\nu_{l2}(a)}_L &= -\frac{1}{8\pi^2} g^{ZhA} \sum_i (y^{\nu Nh}_{l_1 i} y^{\nu NA*}_{l_2,i} + y^{\nu Nh*}_{l_1 i} y^{\nu NA}_{l_2,i}) C_{00}(0,0,m^2_Z, m^2_h, |m_{Ni}|^2, m^2_A) \\ &\quad -\frac{1}{8\pi^2} g^{ZHA} \sum_i (y^{\nu NH}_{l_1 i} y^{\nu NA*}_{l_2,i} + y^{\nu NH*}_{l_1 i} y^{\nu NA}_{l_2,i}) C_{00}(0,0,m^2_Z, m^2_H, |m_{Ni}|^2, m^2_A), \\ \delta g^{\nu_{l1}\nu_{l2}(c)}_L &= \frac{1}{32\pi^2} g^{Z\nu\nu}_L \sum_i (y^{\nu Nh}_{l_1 i} y^{\nu Nh*}_{l_2 i} + y^{\nu Nh*}_{l_1 i} y^{\nu Nh}_{l_2 i}) B_1(0, |m_{Ni}|^2, m^2_h) \\ &\quad + \frac{1}{32\pi^2} g^{Z\nu\nu}_L \sum_i (y^{\nu NH}_{l_1 i} y^{\nu NH*}_{l_2 i} + y^{\nu NH*}_{l_1 i} y^{\nu NH}_{l_2 i}) B_1(0, |m_{Ni}|^2, m^2_H) \\ &\quad + \frac{1}{32\pi^2} g^{Z\nu\nu}_L \sum_i (y^{\nu NA}_{l_1 i} y^{\nu NA*}_{l_2 i} + y^{\nu NA*}_{l_1 i} y^{\nu NA}_{l_2 i}) B_1(0, |m_{Ni}|^2, m^2_A), \\ \delta g^{\nu_{l1}\nu_{l2}}_{L\text{loop}} &= \delta g^{\nu_{l1}\nu_{l2}(a)}_L + \delta g^{\nu_{l1}\nu_{l2}(c)}_L, \end{aligned} \tag{28}$$

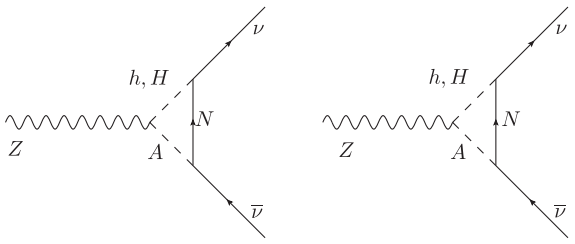

FIG. 3. (a) Diagrams to the $Z-\nu-\bar{\nu}$ vertices.

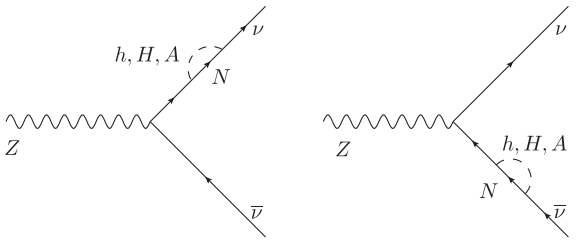

FIG. 4. (c) Diagrams to ν propagators.

where $y_{l_i j}^{\nu N(h,H,A)}$ are the $\nu-N$-neutral Higgs coupling constants after everything is rotated to their mass eigenstates.

In Figs. 1–4. We name the diagram sets "(a)" and "(c)" in order to compare our diagrams and results with Ref. [38], and we should note that "(b)," "(d)," etc., are absent because N_i are SM neutral particles. In Figs. 1 and 2, sterile neutrino propagators are with arrows since they are pseudo-Dirac particles, and the corrections involving μ are omitted.

Despite the loop corrections to the $Z\to\bar{\nu}\nu$ vertices, tree-level shifting due to the mixings between the light neutrinos and the sterile neutrinos should also be considered. Up to the lowest order,

$$\delta g_{L\text{tree}}^{\nu_{l1}\nu_{l2}} = -\delta_{\nu_{l1}\nu_{l2}} g_L^{Z\nu\nu} \sum_i \frac{m_{Dl_1 i}^2}{2m_{Ni}^2}. \tag{29}$$

This is calculated by rotating between the ν_L^w and the N_L^w fields and then comparing the g_L between the different bases. We should note that in order to calculate (29) we need an approximation with a higher order than the V defined in (7), which is rather complicated, so we do not show the detailed process in this paper. In our numerical evaluations, both (28) and (29) are considered.

The definitions of the R_l, A_l, and N_ν are some ratios among expressions of $\bar{g}_{L,R}^{ff}$, or equivalently $\bar{g}_{V,A}^{ff}$. Here, ff include all the lepton and quark pairs. In the model discussed in this paper, the new physics corrections to the Z-quarks couplings from the SM values can be ignored. We also omit the SM-radiative corrections during our evaluations since we only pay attention to the new physics effects. We further define

$$R_{l_i}^{\text{tree}}(\theta_W) = \frac{6[\frac{1}{4}+(\frac{1}{2}-\frac{4\sin^2\theta_W}{3})^2]+9[\frac{1}{4}+(-\frac{1}{2}+\frac{2\sin^2\theta_W}{3})^2]}{\frac{1}{4}+(-\frac{1}{2}+2\sin^2\theta)^2},$$

$$R_{l_i}^{\text{tree}}(\theta_W, g_V^{l_i l_i}, g_A^{l_i l_i}) = \frac{6[\frac{1}{4}+(\frac{1}{2}-\frac{4\sin^2\theta_W}{3})^2]+9[\frac{1}{4}+(-\frac{1}{2}+\frac{2\sin^2\theta_W}{3})^2]}{(g_V^{l_i l_i})^2+(g_A^{l_i l_i})^2},$$

$$A_{l_i}^{\text{tree}}(\theta_W) = -\frac{-\frac{1}{2}+2\sin^2\theta_W}{\frac{1}{4}+(-\frac{1}{2}+2\sin^2\theta_W)^2}$$

$$A_{l_i}^{\text{tree}}(g_V^{l_i l_i}, g_A^{l_i l_i}) = \frac{2g_V^{l_i l_i} g_A^{l_i l_i}}{(g_V^{l_i l_i})^2+(g_A^{l_i l_i})^2}. \tag{30}$$

Calculate Eq. (22) by evaluating the differentials; $\delta R_l = -\frac{\partial R_{l_i}^{\text{tree}}(\theta_W)}{\partial\theta_W} d\theta_W + \frac{\partial R_{l_i}^{\text{tree}}(\theta_W, g_V^{l_i l_i}, g_A^{l_i l_i})}{\partial g_V^{l_i l_i}} dg_V^{l_i l_i} + \frac{\partial R_{l_i}^{\text{tree}}(\theta_W, g_V^{l_i l_i}, g_A^{l_i l_i})}{\partial g_A^{l_i l_i}} dg_A^{l_i l_i}$, and $\delta A_l = -\frac{\partial A_{l_i}^{\text{tree}}(\theta_W)}{\partial\theta_W} d\theta_W + \frac{\partial A_{l_i}^{\text{tree}}(g_V^{l_i l_i}, g_A^{l_i l_i})}{\partial g_V^{l_i l_i}} dg_V^{l_i l_i} + \frac{\partial A_{l_i}^{\text{tree}}(g_V^{l_i l_i}, g_A^{l_i l_i})}{\partial g_A^{l_i l_i}} dg_A^{l_i l_i}$ are given by

$$\delta R_{l_i} = -\frac{4(-19\sin 2\theta_W + 14\sin 4\theta_W + 5\sin 6\theta_W)}{3(2-2\cos 2\theta_W+\cos 4\theta_W)^2}\delta\theta_W + \frac{2(-38+85\cos 2\theta_W - 13\cos 4\theta_W + 11\cos 6\theta_W)}{3(2-2\cos 2\theta_W+\cos 4\theta_W)^2}\delta g_V^{l_i l_i} + \frac{2(36-2\cos 2\theta_W+11\cos 4\theta_W)}{3(2-2\cos 2\theta_W+\cos 4\theta_W)^2}\delta g_A^{l_i l_i}, \tag{31}$$

$$\delta A_{l_i} = \frac{8\sin^2\theta_W \sin 4\theta_W}{(2-2\cos 2\theta_W+\cos 4\theta_W)^2}\delta\theta_W - \frac{8\cos 2\theta_W \sin^2\theta_W}{(2-2\cos 2\theta_W+\cos 4\theta_W)^2}\delta g_V^{l_i l_i} + \frac{8(1-\cos 2\theta_W+\cos 4\theta_W)\sin^2\theta_W}{(2-2\cos 2\theta_W+\cos 4\theta_W)^2}\delta g_A^{l_i l_i}, \tag{32}$$

where the first terms in both Eqs. (31) and (32) originate from the shifting of the G_F, while the rest of the terms indicate the radiative corrections from the charged Higgs loops.

As for δN_ν, things are a little bit subtle. The definition given by Refs. [25,26] is

$$N_\nu^l = \frac{\Gamma_{\text{inv}}^Z}{\Gamma_l^Z}\left(\frac{\Gamma_l^Z}{\Gamma_\nu^Z}\right)_{\text{SM}}, \tag{33}$$

where the $\left(\frac{\Gamma_l^Z}{\Gamma_\nu^Z}\right)_{\text{SM}}$ is used instead of $(\Gamma_\nu)_{\text{SM}}$ in order to reduce the model dependence. However, in our model, both Γ_l and Γ_ν receive corrections. We also define and will calculate

$$N_\nu^{\rm h}=\frac{\Gamma_{\rm inv}^Z}{\Gamma_{\rm h}^Z}\left(\frac{\Gamma_{\rm h}^Z}{\Gamma_\nu^Z}\right)_{\rm SM}, \tag{34}$$

where $\Gamma_{\rm h}^Z$ is the partial width for the $Z\to$ hadrons decay channel, for comparison, since Z-hadron couplings do not receive significant new physics corrections in this model. In the expressions of Eqs. (33) and (34), the SM calculations of $(\frac{\Gamma_{\rm X}^Z}{\Gamma_\nu^Z})_{\rm SM}$ receive shifting from $\delta\theta_W$. $\frac{\Gamma_{\rm inv}^Z}{\Gamma_{\rm X}^Z}$ can be directly extracted from the experimental data, which is controlled by $g_{V,A}$. Since Γ_h^Z does not receive corrections from δg's, unlike Γ_l^Z, δN_ν defined by Eqs. (33) and (34) can be different. Since

$$\begin{aligned}
\frac{\Gamma_{\rm inv}^{Z,\rm tree}}{\Gamma_l^{Z,\rm tree}}&=\frac{\sum_i[(g_V^{\nu_i\nu_i})^2+(g_A^{\nu_i\nu_i})^2]}{\sum_i[(g_V^{l_il_i})^2+(g_A^{l_il_i})^2]}\\
\left(\frac{\Gamma_l^{Z,\rm tree}}{\Gamma_\nu^{Z,\rm tree}}\right)_{\rm SM}&=\frac{3}{2}+6\left(-\frac{1}{2}+2\sin^2\theta_W\right)^2\\
\frac{\Gamma_{\rm inv}^{Z,\rm tree}}{\Gamma_{\rm h}^{Z,\rm tree}}&=\frac{\sum_i[(g_V^{\nu_i\nu_i})^2+(g_A^{\nu_i\nu_i})^2]}{\frac{15}{4}+6(\frac{1}{2}-\frac{4\sin^2\theta_W}{3})^2+9(-\frac{1}{2}+\frac{2\sin^2\theta_W}{3})^2}\\
\left(\frac{\Gamma_{\rm h}^{Z,\rm tree}}{\Gamma_\nu^{Z,\rm tree}}\right)_{\rm SM}&=\frac{15}{2}+12\left(\frac{1}{2}-\frac{4\sin^2\theta_W}{3}\right)^2\\
&\quad+18\left(-\frac{1}{2}+\frac{2\sin^2\theta_W}{3}\right)^2,
\end{aligned} \tag{35}$$

we calculate δN_ν^l and $\delta N_\nu^{\rm h}$ by

$$\begin{aligned}
\delta N_\nu^l&=\left(\frac{\Gamma_l^{Z,\rm tree}}{\Gamma_\nu^{Z,\rm tree}}\right)_{\rm SM}\sum_{g=g_{A,V}^{l/\nu_i,l/\nu_i}}\frac{\partial\frac{\Gamma_{\rm inv}^{Z,\rm tree}}{\Gamma_l^{Z,\rm tree}}}{\partial g}\delta g+\frac{\Gamma_{\rm inv}^{Z,\rm tree}}{\Gamma_l^{Z,\rm tree}}\frac{\partial(\frac{\Gamma_l^{Z,\rm tree}}{\Gamma_\nu^{Z,\rm tree}})_{\rm SM}}{\partial\theta_W}\delta\theta_W,\\
\delta N_\nu^h&=\left(\frac{\Gamma_h^{Z,\rm tree}}{\Gamma_\nu^{Z,\rm tree}}\right)_{\rm SM}\sum_{g=g_{A,V}^{l/\nu_i,l/\nu_i}}\frac{\partial\frac{\Gamma_{\rm inv}^{Z,\rm tree}}{\Gamma_h^{Z,\rm tree}}}{\partial g}\delta g+\frac{\Gamma_{\rm inv}^{Z,\rm tree}}{\Gamma_h^{Z,\rm tree}}\frac{\partial(\frac{\Gamma_h^{Z,\rm tree}}{\Gamma_\nu^{Z,\rm tree}})_{\rm SM}}{\partial\theta_W}\delta\theta_W.
\end{aligned} \tag{36}$$

The results are given by

$$\begin{aligned}
\delta N_\nu^l=&\frac{12(\sin2\theta_W-\sin4\theta_W)}{2-2\cos2\theta_W+\cos4\theta_W}\delta\theta_W+2\sum_i(\delta g_V^{\nu_{li}\nu_{li}}+\delta g_A^{\nu_{li}\nu_{li}})\\
&+\frac{2-8\sin^2\theta_W}{2-2\cos2\theta_W+\cos4\theta_W}\sum_i\delta g_V^{l_il_i}\\
&+\frac{2}{2-2\cos2\theta_W+\cos4\theta_W}\sum_i\delta g_A^{l_il_i},
\end{aligned} \tag{37}$$

$$\begin{aligned}
\delta N_\nu^{\rm h}=&\frac{12(\sin2\theta_W-11\sin4\theta_W)}{36-2\cos2\theta_W+11\cos4\theta_W}\delta\theta_W\\
&+2\sum_i(\delta g_V^{\nu_i\nu_i}+\delta g_A^{\nu_i\nu_i}),
\end{aligned} \tag{38}$$

where $\delta g_{L,R,V,A}^{l_il_j}=\delta g_{L,R,V,A\rm tree}^{l_il_j}+\delta g_{L,R,V,A\rm loop}^{l_il_j}$, and again the first terms in both Eqs. (37) and (38) originate from the shifting of the G_F, while the other terms come from the corrections to the effective $Z-f-\bar f$ corrections, containing both the tree-level and loop-level ones.

We should note that, strictly speaking, "θ_W" in Eqs. (31)–(38) should be replaced by "arcsin(s_l)," which is the angle evaluated from the SM-effective $Z-l-l$ vertices. However, in this paper, we are only concerned with the deviations from the SM predictions, which is insensitive to the definitions of the weak mixing angle, so we do not distinguish them.

The lepton's FCNC decay $\mu\to e\gamma$, $\tau\to\mu\gamma$, $\tau\to e\gamma$ processes together with the muon anomalous $g-2$ provide other windows into the new physics models. All of them involve a one-loop diagram with a charged Higgs boson running inside. The diagram is shown in Fig. 5. We follow the steps in Ref. [40] to calculate the amplitude, which is parametrized by $ie\epsilon_\mu^*(q)M^\mu$, where $e=\sqrt{4\pi\alpha}$ is the coupling constant of the quantum electromagnetic dynamics and ϵ_μ^q is the polarization vector. The definition of M^μ is given by

$$M^\mu=\bar u_2[i\sigma^{\mu\nu}q_\nu(\sigma_{Ll_1l_2}P_L+\sigma_{Rl_1l_2}P_R)u_1, \tag{39}$$

where $P_{L,R}=\frac{1\mp\gamma^5}{2}$ and $\sigma^{\mu\nu}=\frac{i[\gamma^\mu,\gamma^\nu]}{2}$. If $l_1\neq l_2$, the partial width for $f_1\to f_2\gamma$ is given by

$$\Gamma_{l_1\to l_2\gamma}=\frac{(m_{l_1}^2-m_{l_2}^2)^3(|\sigma_{Ll_1l_2}|^2+|\sigma_{Rl_1l_2}|^2)}{16\pi m_{l_1}^3}. \tag{40}$$

If $l_1=l_2$, Eq. (39) also contributes to the anomaly magnetic momenta

$$\delta a_{l_1}=\frac{\sigma_{Ll_1l_1}+\sigma_{Rl_1l_1}}{\frac{e}{2m_{l_1}}}. \tag{41}$$

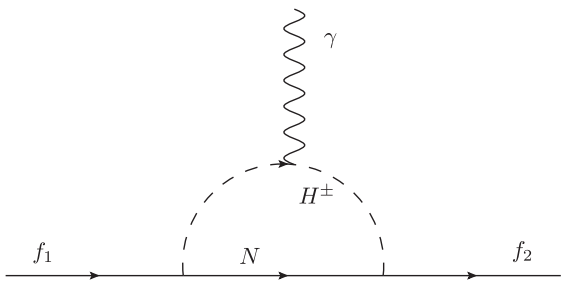

FIG. 5. The diagram for $l_1\to l_2\gamma$. This diagram can also be used to calculate the muon anomalous $g-2$.

Define

$$t_i = \frac{m_{Ni}^2}{m_{H^\pm}^2},$$
$$\bar{c}_{1,i} = \bar{c}_{2,i} = \frac{1}{16\pi^2 m_{H^\pm}^2}\left[\frac{3t_i - 1}{4(t_i-1)^2} - \frac{t_i^2 \ln t_i}{2(t_i-1)^3}\right],$$
$$\bar{d}_{1,i} = \bar{d}_{2,i} = 2\bar{f}_i = \frac{1}{16\pi^2 m_{H^\pm}^2}\left[\frac{11t_i^2 - 7t_i + 2}{18(t_i-1)^3} - \frac{t_i^3 \ln t_i}{3(t_i-1)^4}\right],$$
$$\lambda_{l_1 l_2 i} = y^*_{Nl_2 i} y_{Nl_1 i},$$
(no Einstein summation rules for the index i),
$$\bar{k}_{1,l_1 l_2 i} = m_{l_1}(-\bar{c}_1 + \bar{d}_1 + \bar{f}),$$
$$\bar{k}_{2,l_1 l_2 i} = m_{l_2}(-\bar{c}_2 + \bar{d}_2 + \bar{f}). \quad (42)$$

Then, the $\sigma_{L,Rl_1 l_2}$ are given by

$$\sigma_{L,l_1,l_2} = Q_B \lambda \bar{k}_2,$$
$$\sigma_{R,l_1,l_2} = Q_B \lambda \bar{k}_1. \quad (43)$$

By taking Eq. (43) to Eqs. (40) and (41), we can then calculate the partial widths of the FCNC decay of the $\mu \to e\gamma$, $\tau \to \mu\gamma$, $\tau \to e\gamma$ processes together with the muon anomalous $g-2$.

IV. NUMERICAL CALCULATIONS AND RESULTS

In this section, we are going to show the results of δR_{l_i}, δA_{l_i}, and δN_ν together with the bounds from $\mu \to e\gamma$, $\tau \to \mu\gamma$, and $\tau \to e\gamma$ in each case listed in Table I. The muon's anomalous $g-2$ is also considered.

Since we are mainly concerned with the Z-resonance observables involving the leptons, the interactions among the Higgs sectors are less important. Under the $\tan\beta \to \infty$ limit and the alignment limit $\sin(\beta-\alpha) \to 1$, only the mass spectrum of the Higgs bosons and the sterile neutrinos, together with their Yukawa coupling constants, play the key roles in resolving the observables. The left-handed neutrino mass spectrum and their mixing patterns are also the input parameters for calculating the mass spectrum of the sterile neutrinos and their Yukawa couplings. After adopting the data in (13) and ignoring all the CP phases, we still need the lightest neutrino mass $m_{\nu 0}$ to determine the complete neutrino mass spectrum. Both the normal ordering $m_1 < m_2 < m_3$ and the inverse ordering $m_3 < m_1 < m_2$ are calculated; however, only the results for the normal ordering are presented since there is no significant difference between these two orderings.

Despite the light neutrino mass and mixing parameters, m_N and m_D can be characterized by the lightest sterile neutrino's mass m_{N0} and the largest SM-effective $y_{\rm SM}^{\rm max}$. The $y_{\rm SM}^{\rm max}$ is defined by the value of the element with the smallest absolute value in the SM-effective coupling matrix $Y_N \cos\beta$. Besides, $m_{H^\pm}$ determines R_{l_i} and A_{l_i}, while $m_{H,A}$ also affect $N_{\delta\nu}$. In this paper, we fix $m_h = 125$ GeV.

As for the $l_1 \to l_2\gamma$ bounds, we adopt the data from Refs. [25,41–43],

$$\mathrm{Br}_{\mu\to e\gamma} < 4.2 \times 10^{-13},$$
$$\mathrm{Br}_{\tau\to\mu\gamma} < 4.4 \times 10^{-8},$$
$$\mathrm{Br}_{\tau\to e\gamma} < 3.3 \times 10^{-8}. \quad (44)$$

The Planck Collaboration also gives constraints on the summation of the light neutrino mass [44]:

$$\sum_i m_{\nu_i} < 0.23 \text{ eV}. \quad (45)$$

The deviation of the muon's anomalous magnetic momenta between the experimental and the theoretical evaluation results is $\delta a_\mu = 288(63)(49) \times 10^{-11}$ [25,28–30]. Here, we adopt the $3-\sigma$ range of

$$48.56 \times 10^{-11} < \delta a_\mu < 527.44 \times 10^{-11}. \quad (46)$$

Since in many cases the differences between δN_ν^l and $\delta N_\nu^{\rm h}$ are not very significant, we refer to δN_ν^l when we refer to δN_ν.

We should also note that we have used 2HDMC-1.7.0 [45] to help us calculate various intermediate variables.

The results of case 1 are presented in Fig. 6. Here, $m_H = m_{H^\pm} = m_A = 200$ GeV. $\tan\beta = 1000$, $\sin(\beta-\alpha) = 0.9999$, and $m_{N_0} = 20$ GeV. Figure 6 clearly shows that most of the parameter space has been excluded by the $\mu \to e\gamma$ and the Planck $\sum_i m_{\nu_i}$ bounds. The deviation of the muon anomalous magnetic momenta $g-2$ cannot be explained while satisfying the $l_1 \to l_2\gamma$ bounds.

The results of case 2 are presented in Fig. 7. Compared with case 1, the $\mu \to e\gamma$ bounds are somehow relaxed but are, however, still far from explaining the deviation of the muon's anomalous magnetic momenta.

In case 1 and case 2, we can give rise to either of the m_{N0} or $m_{H^\pm}$ in order to suppress the branching ratio of $l_1 \to l_2\gamma$. However, δR_{l_i}, δA_{l_i}, and δN_ν will also be lowered, making it more difficult to test in the future Z-resonance experiments.

As for case 3, $l_1 \to l_2\gamma$ originating from the new physics sectors can be omitted. In this case, all the leptonic FCNC effects come from the matrix μ. Up to the lowest order, the diagram in Fig. 8 contains two insertions of μ, suppressing the $l_1 \to l_2\gamma$ branching ratio by a factor of $(\frac{\mu}{m_N})^4$. The complete formula is too lengthy to present in this paper; however, in the special case in which $m_N = m_{H^\pm} = M$, we have

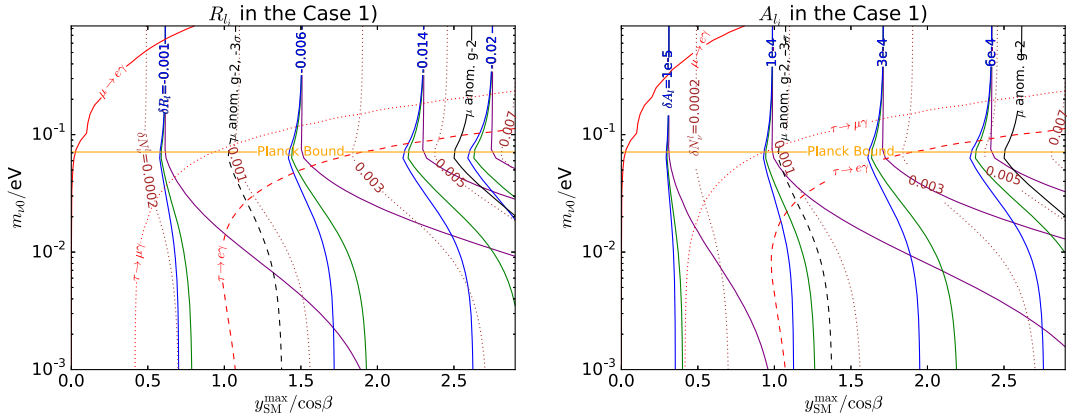

FIG. 6. R_{l_i} (left panel) and A_{l_i} (right panel) together with the $l_1 \to l_2\gamma$ bounds and the 3-$\sigma g-2$ range. Here, $m_H = m_{H^\pm} = m_A = 200$ GeV. $\tan\beta = 1000$, $\sin(\beta-\alpha) = 0.9999$, and $m_{N_0} = 20$ GeV. The purple, green, and blue lines indicate $\delta R/\delta A_{e,\mu,\tau}$, respectively. As for the $l_i \to l_j\gamma$ constraints, the lower area has been excluded, and as for the "Planck bound" constraint, the upper area has been excluded.

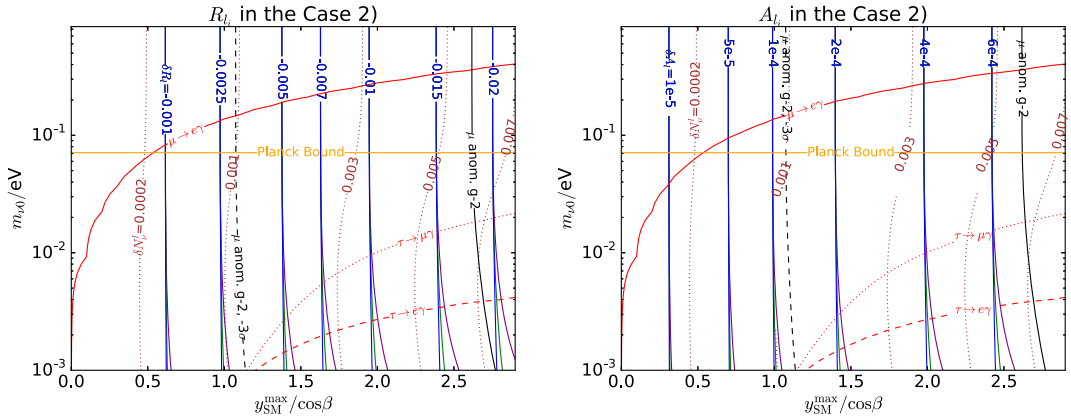

FIG. 7. R_{l_i} (left panel) and A_{l_i} (right panel) together with the $l_1 \to l_2\gamma$ bounds and the 3-$\sigma g-2$ range. Here, $m_H = m_{H^\pm} = m_A = 200$ GeV. $\tan\beta = 1000$, $\sin(\beta-\alpha) = 0.9999$, and $m_{N_0} = 20$ GeV. The purple, green, and blue lines indicate $\delta R/\delta A_{e,\mu,\tau}$, respectively. As for the $l_i \to l_j\gamma$ constraints, the lower area has been excluded, and as for the Planck bound constraint, the upper area has been excluded.

$$\sigma_{L,l_1,l_2} = \frac{m_{l_2} y_N \sum_i \mu_{l_1 i}\mu_{l2i}}{1920\pi^2 M^4},$$
$$\sigma_{R,l_1,l_2} = \frac{m_{l_1} y_N \sum_i \mu_{l_1 i}\mu_{l2i}}{1920\pi^2 M^4}, \tag{47}$$

where y_N is the diagonal element of $Y_N \propto I$ and where $l_1 \neq l_2$. Compared with case 1 and 2, the new physics contributions to the $l_1 \to l_2\gamma$ amplitude are too small, so we do not discuss them in case 3.

The results of δR_l and δA_l together with the $3-\sigma$ muon's anomalous magnetic momenta range are presented in Figs. 9, 10, and 11. The model's parameter values other than the axis titles are shown in the figure captions. Notice that in case 3 the difference between $R_{e,\mu,\tau}$ and $A_{e,\mu,\tau}$ is very small, so we do not distinguish them in the figures.

Compare Figs. 9 and 10; it is obvious that the rise of m_N suppresses the values of R_l and A_l. As for δN_ν, in most of the cases, $\delta N_\nu > 0$ because the positive one-loop contribution dominates. However, when m_N is small, sometimes the tree-level mixing effects between the light neutrinos and the sterile neutrinos dominate. In this case, $\delta N_\nu < 0$. This is more obvious when comparing Fig. 9 with Fig. 11. In

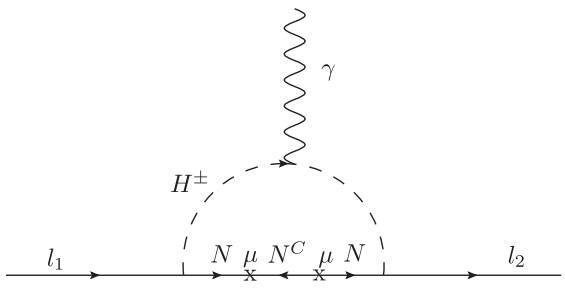

FIG. 8. $l_1 \to l_2\gamma$ diagram up to the lowest order in case 3.

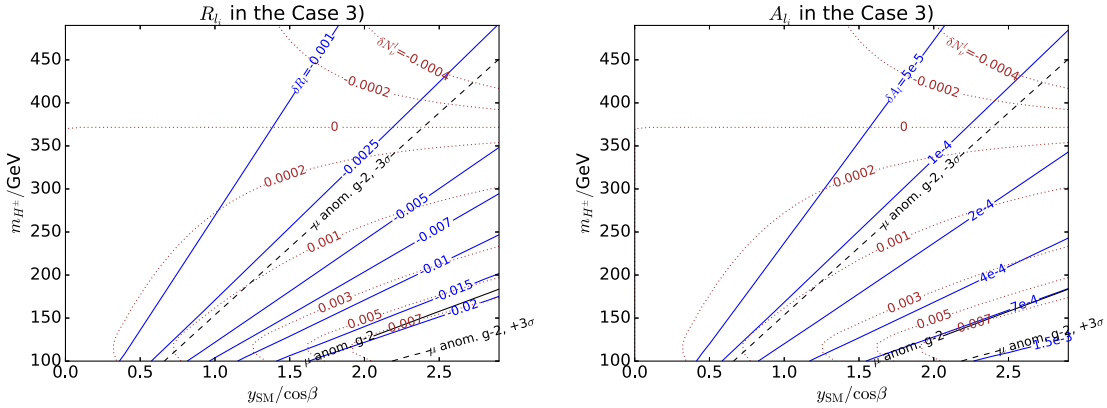

FIG. 9. R_{l_i} (left panel) and A_{l_i} (right panel) together with the $3-\sigma g-2$ range. Here, $m_H = m_{H^\pm} = m_A$ when $m_{H^\pm} > 125$ GeV; however, $m_H = 125.1$ GeV and $m_{H^\pm} = m_A$ when $m_{H^\pm} < 125$ GeV. $\tan\beta = 1000$, $\sin(\beta-\alpha) = 0.9999$, and $m_{N_0} = 20$ GeV.

Fig. 11, $y_{\rm SM}$ is relatively larger due to the smaller $\tan\beta$; therefore, the tree-level mixing effects always dominate so that $\delta N_\nu < 0$. The significant difference of δA_l between Figs. 9 and 11 in the large $y_{\rm SM}/\cos\beta$ area is due to the shifting of θ_W formulated in (21), which becomes more significant when the mixings between the light neutrinos and the sterile neutrino arise.

Although in the previous discussions usually $\frac{\delta N_\nu^l}{\delta N_\nu^{\rm h}} \approx 1$, this is not always the truth. Compared with δN_ν^l, $\delta N_\nu^{\rm h}$ only receives the corrections from the neutral Higgs bosons in the one-loop level. In the limit that $m_H, m_A \to \infty$ while $m_{H^\pm}$ remains small, δN_ν^l still receive large loop corrections due to the shifting of Γ_l, while in this case, $\delta N_\nu^{\rm h}$ only receives tree-level corrections; then, large deviations between $\frac{\delta N_\nu^l}{\delta N_\nu^{\rm h}}$ and 1 arise. Figure 12 can reflect this fact in a specific area of the parameter space.

V. DISCUSSIONS

Current experiment results show an absolute uncertainty of ~0.03–0.05 in the measurement of $R_{e,\mu,\tau}$ and an absolute uncertainty of ~0.005 in the measurement of $A_{e,\mu,\tau}$ [25], which is far from testing or constraining this model compared with the predicted $\delta R_{l_i}/\delta A_{l_i}$. On the future colliders, the CEPC-PreCDR [46] has mentioned that the uncertainty of R_μ can be improved by a factor of roughly $\frac{1}{5}$. Neither the Pre-CDR of the CEPC nor ILC-GigaZ chapter in the ILC-TDR [47] gives the data for other parameters. However, it is reasonable to expect all these will be improved by roughly a of factor $\frac{1}{5}$, which can then be compared with the predicted $\delta R_{l_i}/\delta A_{l_i}$ in some of the parameter space. On the FCC-ee, Refs. [48,49] showed that the uncertainty of R_{l_i} can reach 0.001, while the uncertainty of A_{l_i} was not mentioned. However, $A_{FB}^{\mu\mu}$ can reach a relative uncertainty of 0.023%, which can result in a similar relative uncertainty of A_l with the assumption of $A_e = A_\mu$ and the formula $A_{FB}^{\mu\mu} = \frac{3}{4}A_e A_\mu$. Therefore, the performances of R_l and A_l on the FCC-ee are enough to cover much of the parameter space as shown in Figs. 9, 10, and 11. The new Z factory proposed in Ref. [50] did not mention the measured precision of the Z-resonance parameters directly. However, comparing the luminosity data

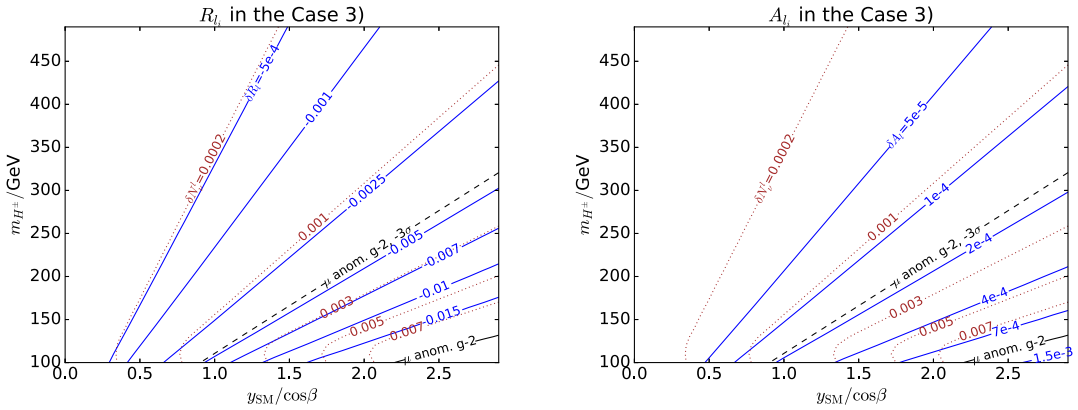

FIG. 10. R_{l_i} (left panel) and A_{l_i} (right panel) together with the $3-\sigma g-2$ range. Here, $m_H = m_{H^\pm} = m_A$ when $m_{H^\pm} > 125$ GeV; however, $m_H = 125.1$ GeV and $m_{H^\pm} = m_A$ when $m_{H^\pm} < 125$ GeV. $\tan\beta = 1000$, $\sin(\beta-\alpha) = 0.9999$, and $m_{N_0} = m_{H^\pm}$.

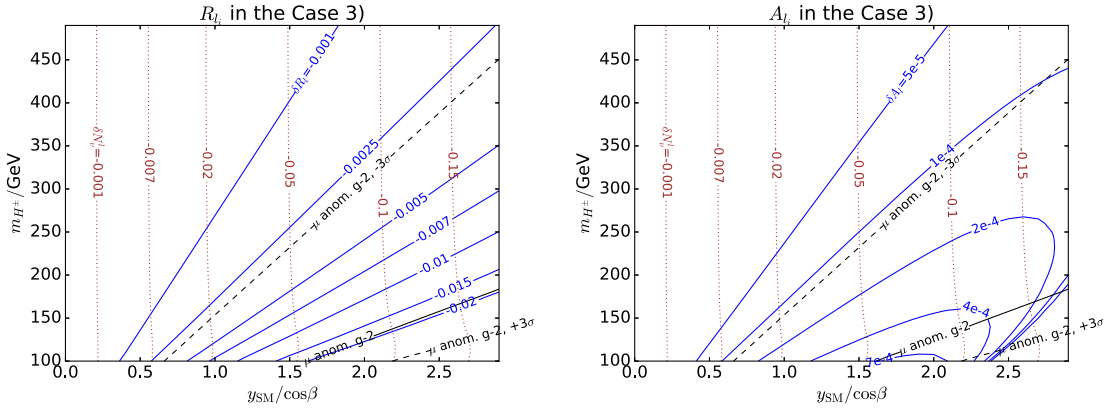

FIG. 11. R_{l_i} (left panel) and A_{l_i} (right panel) together with the $3-\sigma g-2$ range. Here, $m_H = m_{H^\pm} = m_A$ when $m_{H^\pm} > 125$ GeV; however, $m_H = 125.1$ GeV and $m_{H^\pm} = m_A$ when $m_{H^\pm} < 125$ GeV. $\tan\beta = 300$, $\sin(\beta-\alpha) = 0.9999$, and $m_{N_0} = 20$ GeV.

given in Ref. [50] with Ref. [48], it is reasonable to expect a similar number of Z bosons can be produced in both of the two proposals. Therefore, a similar measured precision of the Z-resonance parameters can be reached.

Another challenge is the uncertainties of the theoretical predictions of R_l and A_l. Currently, the theoretical uncertainty of R_l is dominated by α_s, which appears in the calculations of Γ_h. To avoid a circular argument, we cannot use the α_s extracted from the Z-resonance measurements. However, in Ref. [51], Large Hadron electron Collider (LHeC) itself has the potential to improve α_s by an order of magnitude, which will also improve the calculations of R_l. As for A_l, the uncertainty mainly originates from the effective weak mixing angle $\sin^2\theta_l$. This depends on all the SM parameters, including α, the fine structure constant, and the Z-boson mass m_Z. As for α, if the future fittings of the uncertainty of $\Delta\alpha^{(5)}_{\rm had}(M_Z^2)$ (for a review about this parameter, see Ref. [25]; for an example calculating this from experimental data, see Ref. [52]) can be improved by a factor of $\frac{1}{2}-\frac{1}{5}$, together with all the uncertainties of other SM parameters (including m_Z) improved by an order of magnitude, the uncertainty of theoretical A_l can also be improved and can be compared with much of the parameter space in Figs. 9, 10, and 11.

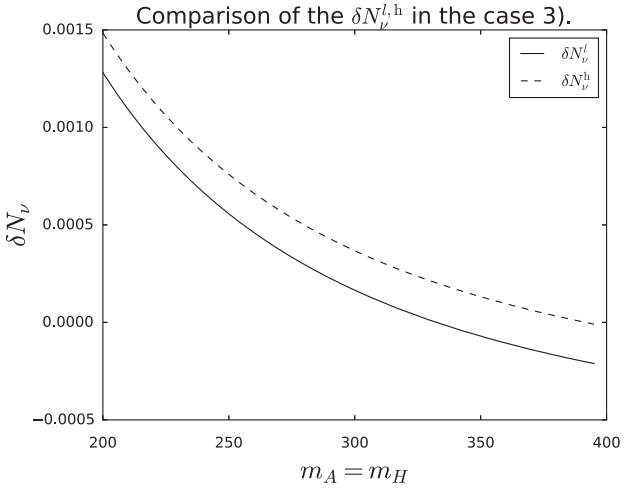

FIG. 12. Comparison of the $\delta N_\nu^{l,h}$. Here, $m_H = m_A$ $m_{H^\pm} = 200$ GeV, $\tan\beta = 1000$, $\sin(\beta-\alpha) = 0.9999$, $m_{N_0} = 20$ GeV, and $y_{SM}/\cos\beta = 1.5$.

On the future colliders, the on-shell $H^\pm$ might be directly produced and then decay dominantly into $l^\pm + N$ in this model, and N then cascade decay into various SM objects that can be detected. Reference [14] discussed this channel on the future High Luminosity Large Hadron Collider (HL-LHC). Their result is the 100 GeV $\lesssim m_N < m_{H^\pm} \lesssim$ 500 GeV can be constrained in the future. However, heavy $m_{H^\pm} \gtrsim 100$ GeV with a rather small $m_N \ll 100$ GeV have not been discussed. The nearly degenerate $m_N \approx m_{H^\pm}$ case is also difficult to constrain. That is part of the reason why we have only presented the result when $m_N = 20$ GeV or $m_N = m_{H^\pm}$ in Sec. IV. Interestingly, we should note that when $m_N \ll m_{H^\pm}$ the sterile neutrino N decays into collinear objects, which is worth studying in the future.

VI. CONCLUSIONS

We proposed the νTHDM with the inverse seesaw mechanisms. The Yukawa coupling involving the sterile neutrinos and the exotic Higgs bosons can take the value of order 1. We have calculated the electroweak parameters R_l and A_l. The $l_1 \to l_2\gamma$ bounds are considered, and we also calculated the predicted muon anomalous momenta $g-2$. Three cases in the Table I together with the flavor stuctures of the neutrinos have been considered. Large areas of the parameter space in case 1 and case 2 are excluded by the $\mu \to e\gamma$ bound and the Planck constraint on $\sum_i m_{\nu_i}$. However, case 3 does not receive a large correction from the new physics in FCNC parameters. By comparing the theoretical evaluations and the plans for the future collider experiments, the deviation of R_l and A_l from the SM predicted values can be tested in the future collider (especially the FCC-ee) experiments.

ACKNOWLEDGMENTS

We would like to thank Chen Zhang, Jue Zhang, Ran Ding, and Arindam Das for helpful discussions. This work was supported in part by the Natural Science Foundation of China (Grants No. 11135003, No. 11635001, and No. 11375014) and by the China Postdoctoral Science Foundation under Grant No. 2016M600006.

[1] P. Minkowski, Phys. Lett. **67B**, 421 (1977).
[2] T. Yanagida, in *Proceedings of the Workshop on Unified Theory and Baryon Number of the Universe* (KEK, Tsukuba, Japan, 1979), p. 95.
[3] P. R. M. Gell-Mann and R. Slansky, in *Sanibel talk, CALT-68-709 (Feb. 1979), and in Supergravity* (North Holland, Amsterdam, 1979), p. 315.
[4] S. Glashow, *Quarks and Leptons* (Plenum, New York, 1980), p. 707.
[5] R. N. Mohapatra and G. Senjanovic, Phys. Rev. Lett. **44**, 912 (1980).
[6] D. Wyler and L. Wolfenstein, Nucl. Phys. **B218**, 205 (1983).
[7] R. N. Mohapatra and J. W. F. Valle, Phys. Rev. D **34**, 1642 (1986).
[8] E. Ma, Phys. Lett. B **191**, 287 (1987).
[9] R. N. Mohapatra, Phys. Rev. Lett. **56**, 561 (1986).
[10] P. Humbert, M. Lindner, and J. Smirnov, J. High Energy Phys. 06 (2015) 035.
[11] E. Ma, Phys. Rev. Lett. **86**, 2502 (2001).
[12] S. Gabriel and S. Nandi, Phys. Lett. B **655**, 141 (2007).
[13] N. Haba and K. Tsumura, J. High Energy Phys. 06 (2011) 068.
[14] C. Guo, S.-Y. Guo, Z.-L. Han, B. Li, and Y. Liao, J. High Energy Phys. 04 (2017) 065.
[15] S. M. Davidson and H. E. Logan, Phys. Rev. D **80**, 095008 (2009).
[16] E. Bertuzzo, Y. F. Perez, G. O. Sumensari, and R. Zukanovich Funchal, J. High Energy Phys. 01 (2016) 018.
[17] W. Wang and Z.-L. Han, Phys. Rev. D **94**, 053015 (2016).
[18] P. A. N. Machado, Y. F. Perez, O. Sumensari, Z. Tabrizi, and R. Z. Funchal, J. High Energy Phys. 12 (2015) 160.
[19] F. Wang, W. Wang, and J. M. Yang, Europhys. Lett. **76**, 388 (2006).
[20] G. C. Branco, P. M. Ferreira, L. Lavoura, M. N. Rebelo, M. Sher, and J. P. Silva, Phys. Rep. **516**, 1 (2012).
[21] B. Świeżewska, Phys. Rev. D **88**, 055027 (2013); **88**, 119903(E) (2013).
[22] D. Das, Int. J. Mod. Phys. A **30**, 1550158 (2015).
[23] D. Das and I. Saha, Phys. Rev. D **91**, 095024 (2015).
[24] A. Castillo, R. A. Diaz, J. Morales, and C. G. Tarazona, arXiv:1607.07972.
[25] C. Patrignani *et al.* (Particle Data Group), Chin. Phys. C **40**, 100001 (2016).
[26] S. Schael *et al.* (SLD Electroweak Group, DELPHI, ALEPH, SLD, SLD Heavy Flavour Group, OPAL, LEP Electroweak Working Group, and L3 Collaborations), Phys. Rep. **427**, 257 (2006).
[27] L. E. W. Group (Tevatron Electroweak Working Group, CDF, DELPHI, SLD Electroweak Group, Heavy Flavour Group, ALEPH, LEP Electroweak Working Group, SLD, OPAL, D0, and L3 Collaborations), arXiv:1012.2367.
[28] J. P. Miller, E. de Rafael, and B. L. Roberts, Rep. Prog. Phys. **70**, 795 (2007).
[29] F. Jegerlehner and A. Nyffeler, Phys. Rep. **477**, 1 (2009).
[30] J. P. Miller, E. de Rafael, B. L. Roberts, and D. Stöckinger, Annu. Rev. Nucl. Part. Sci. **62**, 237 (2012).
[31] S. Antusch and O. Fischer, J. High Energy Phys. 10 (2014) 094.
[32] F. Capozzi, E. Lisi, A. Marrone, D. Montanino, and A. Palazzo, Nucl. Phys. **B908**, 218 (2016).
[33] M. Hirsch, S. Morisi, and J. W. F. Valle, Phys. Lett. B **679**, 454 (2009).
[34] B. Karmakar and A. Sil, Phys. Rev. **96**, 015007 (2017).
[35] D. M. Webber *et al.* (MuLan Collaboration), Phys. Rev. Lett. **106**, 041803 (2011); **106**, 079901 (2011).
[36] J. M. Roney, Nucl. Phys. B, Proc. Suppl. **169**, 379 (2007).
[37] T. Fukuyama and K. Tsumura, arXiv:0809.5221.
[38] H. E. Haber and H. E. Logan, Phys. Rev. D **62**, 015011 (2000).
[39] T. Hahn and M. Perez-Victoria, Comput. Phys. Commun. **118**, 153 (1999).
[40] L. Lavoura, Eur. Phys. J. C **29**, 191 (2003).
[41] J. Adam *et al.* (MEG Collaboration), Phys. Rev. Lett. **110**, 201801 (2013).
[42] A. M. Baldini *et al.* (MEG Collaboration), Eur. Phys. J. C **76**, 434 (2016).
[43] B. Aubert *et al.* (*BABAR* Collaboration), Phys. Rev. Lett. **104**, 021802 (2010).
[44] P. A. R. Ade *et al.* (Planck Collaboration), Astron. Astrophys. **594**, A13 (2016).
[45] D. Eriksson, J. Rathsman, and O. Stal, Comput. Phys. Commun. **181**, 189 (2010).
[46] CEPC-SPPC Study Group, Report Nos. IHEP-CEPC-DR-2015-01, IHEP-TH-2015-01, IHEP-EP-2015-01, 2015, http://cepc.ihep.ac.cn/preCDR/volume.html.
[47] H. Baer *et al.*, arXiv:1306.6352.
[48] M. Dam, arXiv:1601.03849.
[49] P. Janot, J. High Energy Phys. 02 (2016) 053.
[50] C. C. JianPing Ma, Sci. China: Phys., Mech. Astron. **53**, 1947 (2010).
[51] J. L. Abelleira Fernandez *et al.* (LHeC Study Group Collaboration), J. Phys. G **39**, 075001 (2012).
[52] M. Davier, A. Hoecker, B. Malaescu, and Z. Zhang, Eur. Phys. J. C **71**, 1 (2011); **72**, 1874(E) (2012).